Enhanced Charge-Carrier Injection and Collection Via Lamination of Doped Polymer Layers p-Doped with a Solution-Processible Molybdenum Complex

*An Dai, Yinhua Zhou, Andrew L. Shu, Swagat K. Mohapatra, He Wang, Canek Fuentes-Hernandez, Yadong Zhang, Stephen Barlow, Yueh-Lin Loo, Seth R. Marder, Bernard Kippelen, and Antoine Kahn**

Poly(3-hexylthiophene) (P3HT) is p-doped by the new soluble dopant molybdenum tris[1-(methoxycarbonyl)-2-(trifluoromethyl)-ethane-1,2-dithiolene] and investigated via photoemission spectroscopy and transport measurements. Soft-contact transfer lamination of thin layers of the doped P3HT on undoped polymer layers is used to create spatially-confined doped regions, which serve as hole-injection contacts on P3HT diodes. This strategy is then used to create efficient hole-collecting contacts on solution-processed inverted polymer solar cells.

1. Introduction

Engineering molecular-level alignment at electrode/organic interfaces in order to achieve efficient charge injection or collection has generated considerable activity in the field of organic electronics, where contacts directly affect device performance.[1–10] In inorganic semiconductors, Ohmic contacts are often enabled by degenerate doping of the semiconductor at the contact interface, to induce a narrow depletion region through which carriers can effectively tunnel.[11] Similar strategies have been successfully applied to vacuum-deposited small-molecule organic thin films, in which the width of a heavily doped region can be straightforwardly controlled down to a few nanometers by co-evaporation of the host and the dopant molecules.[2,4,12,13] Carrier injection enhancement of several orders-of-magnitude in organic light-emitting diodes and transistors has been demonstrated.[14–18] Doping-induced enhancement of charge carrier collection at small-molecule organic solar cell contacts has also been demonstrated.[12,13,19]

Achieving the same degree of spatial control of dopant profile for polymer-based devices is more challenging: polymer films are solution-deposited and, although doped films can be obtained via deposition of a solution containing the host and dopant, spatial distribution of the dopants cannot be easily controlled. Sequential spin-coating of undoped and doped films using orthogonal solvents is one possible approach; however, the polymer–solvent compatibility needed for forming high quality films and interfaces is not assured. We present here a conceptually simple approach based on soft-contact transfer-lamination (SCTL) of a polymer homojunction, using a soft stamp, for example, polydimethylsiloxane (PDMS), as a transfer medium. SCTL has been extensively used in the past for the deposition of metal electrodes[20,21] or active layers in organic transistors[22,23] and photovoltaic cells.[24–28] In the present case, two polymer films, one undoped and one doped, are prepared separately via spin-coating, and then joined via SCTL to realize doped hole-injection or -collection contacts for diodes and solar cells. We have previously demonstrated with two polymers, poly(3-hexylthiophene) (P3HT) (**Figure 1**) and poly[(9-,9-dioctylfluorenyl-2,7-diyl)-co-(1,4-benzo-{2,1′-3}-thiadiazole)] (F8BT), that the lamination process of undoped films leads to "transparent" homojunctions, that is, interfaces that are electronically and electrically seamless[29] as evidenced by the facts that i) no significant energy shift of molecular levels occurs across the SCTL junction, and ii) the current injected from either electrode is independent of whether the middle layer consists of a single polymer film of thickness *"t"*, or of two laminated films with the same total thickness *"t"*. These results demonstrate that SCTL is a viable method for assembling multilayer polymer devices from separately fabricated layers, thus enabling functionalization, doping, and other materials modification of specific parts of a device structure. Though demonstrated to work effectively across metal-metal interfaces, this

A. Dai, A. L. Shu, H. Wang, Prof. A. Kahn
Department of Electrical Engineering
Princeton University
Princeton, NJ, 08544, USA
E-mail: kahn@princeton.edu
Dr. Y. Zhou, Dr. C. Fuentes-Hernandez,
Prof. B. Kippelen
Center for Organic Photonics and Electronics (COPE)
School of Electrical and Computer Engineering
Georgia Institute of Technology
Atlanta, GA, 30332–0400, USA
Dr. S. K. Mohapatra, Dr. Y. Zhang, Dr. S. Barlow, Prof. S. R. Marder
School of Chemistry and Biochemistry
Georgia Institute of Technology
Atlanta, GA, 30332–0400, USA
H. Wang, Prof. Y.-L. Loo
Department of Chemical and Biological Engineering
Princeton University
Princeton, NJ, 08544, USA

DOI: 10.1002/adfm.201303232

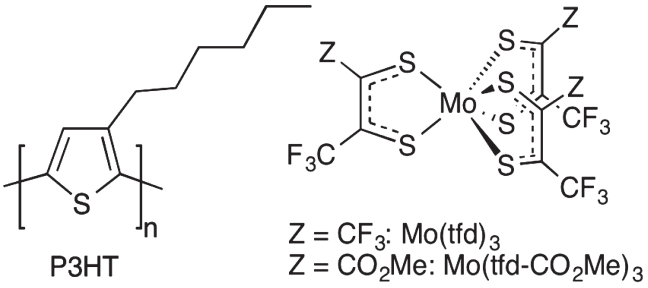

Figure 1. Chemical structures of the host material P3HT and the dopant Mo(tfd-CO_2Me)$_3$.

type of lamination procedure is precluded for inorganic semiconductors, as dangling bonds would introduce considerable densities of interface traps and recombination centers.

We were interested in extending the soft-lamination concept to the fabrication of doped/undoped junctions using the hole-transport material P3HT. Initial attempts to use the strong oxidant molybdenum tris-[1,2-bis(trifluoromethyl)ethane-1,2-dithiolene] (Mo(tfd)$_3$),[4] which can easily be incorporated via co-evaporation in, and efficiently p-dopes, molecular hosts, such as N,N′-di-[(1-naphthyl)-N,N′-diphenyl]-1,1′-biphenyl)-4,4′-diamine(α-NPD) (ionization energy IE = 5.4 eV[4]) were complicated by its tendency to give extensive precipitation when mixed with solutions of polymers like P3HT, making the formation of well-controlled doped films nearly impossible. We therefore designed a new derivative of this dopant bearing more solubilizing groups: molybdenum tris-[1-(methoxycarbonyl)-2-(trifluoromethyl) ethane-1,2-dithiolene (Mo(tfd-CO_2Me)$_3$) (Figure 1). Here we report the synthesis, ionization energy (IE) and electron affinity (EA), and use in doping of P3HT, of Mo(tfd-CO_2Me)$_3$. We then demonstrate SCTL of undoped and doped P3HT films, and the desired current injection enhancement. Finally, we create efficient hole-collection contacts on bulk heterojunction solar cells using this same approach.

2. Design, Synthesis, and Characterization of Mo(tfd-CO_2Me)$_3$

We attributed the poor solubility encountered when preparing Mo(tfd)$_3$-doped P3HT to the symmetry and rigidity of the Mo(tfd)$_3$ anion and the poorly solubilizing effects of the fluoroalkyl substituents. We hypothesized that replacement of one of the trifluoromethyl groups of each dithiolene ligand with an alkyl ester would increase the degrees of freedom in the complex and also decrease unfavorable fluoroalkyl-hydrocarbon interactions, while, at the same time, the electron-withdrawing characteristics of the ester group would help maintain a high EA in the complex. The dianion of Mo(tfd-CO_2Me)$_3$ was isolated as its tetraethylammonium salt from the reaction of methyl 4,4,4-trifluorobut-2-ynoate)[30] with $(NEt_4^+)_2[MoS_9]^{2-}$;[31] the neutral dopant was obtained after oxidation of the dianion with nitrosonium hexafluorophosphate. As well as facilitating solution-processing of doped polymer (see below), the ester substituents of Mo(tfd-CO_2Me)$_3$ also lead to considerably increased solubility for the neutral dopant (e.g., ca. 50 mg/mL in chlorobenzene) over that of Mo(tfd)$_3$ (ca. 3 mg mL^{-1} in the same solvent). More details on the synthesis are given in the experimental section.

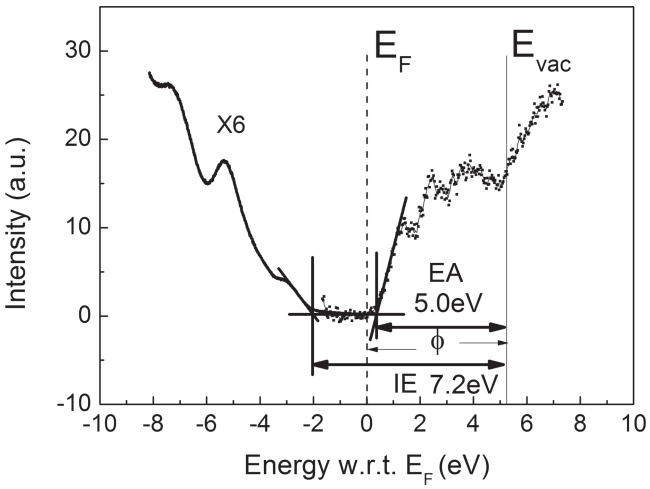

Figure 2. Combined UPS (left) and IPES (right) spectra of Mo(tfd-CO_2Me)$_3$ film. The Fermi level (E_F) is the reference 0 eV. The onsets of occupied and unoccupied states with respect to the vacuum level (E_{vac}) yield IE = 7.2 eV and EA = 5.0 eV, respectively.

The IE and EA of Mo(tfd-CO_2Me)$_3$ was determined from ultrahigh vacuum ultraviolet and inverse photoemission spectroscopy (UPS, IPES), respectively, of a film spin-coated on Au (**Figure 2**). From the UPS spectrum, the IE of the film, conventionally defined as the difference between the vacuum level (E_{vac}) and the onset of the highest occupied molecular orbital (HOMO) is 7.2 eV. The EA, determined from the IPES spectrum as the difference between E_{vac} and the onset of the lowest unoccupied molecular orbital (LUMO), is 5.0 eV. Although the EA is 0.6 eV smaller than that of Mo(tfd)$_3$,[4] indicating that Mo(tfd-CO_2Me)$_3$is a weaker oxidant, it is still sufficiently large for p-doping P3HT, which has an IE of 4.65 eV.[32]

3. Doped P3HT Films

3.1. Electronic Structure

UPS spectra of the HOMO region of P3HT films doped with increasing concentrations of Mo(tfd-CO_2Me)$_3$ are shown in **Figure 3**. The 20 nm-thick P3HT films were spin-coated on cleaned ITO substrates and annealed in nitrogen at 110 °C for 10 min. The figure shows the progressive shift of the HOMO edge toward the Fermi level (E_F = 0 eV), as expected for p-doping. Note that 1 wt% of Mo(tfd-CO_2Me)$_3$ in P3HT corresponds to about 1 dopant molecule for every 450 P3HT thiophene mers. The energy difference between the Fermi level and the HOMO edge decreases from 0.70 eV for the undoped film to 0.61, 0.44, and 0.32 eV for 1, 4, and 10 wt% doping level, respectively. Concomitantly, the work function (WF) of the film increases from 4.0 to 4.15, 4.26, and 4.5 eV for the same doping concentration values. Note that, although close, the WF change does not strictly mirror the Fermi level shift, as the IE and EA

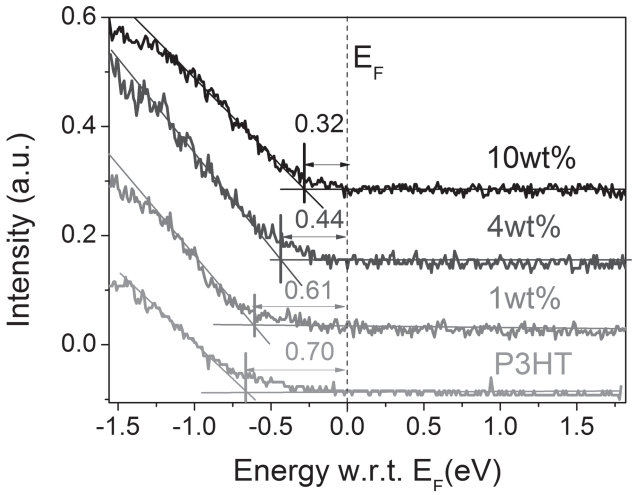

Figure 3. He I UPS spectra of the HOMO region of P3HT as a function of Mo(tfd-CO_2Me)$_3$ doping concentration. The Fermi level shifts towards the HOMO edge as the doping concentration increases.

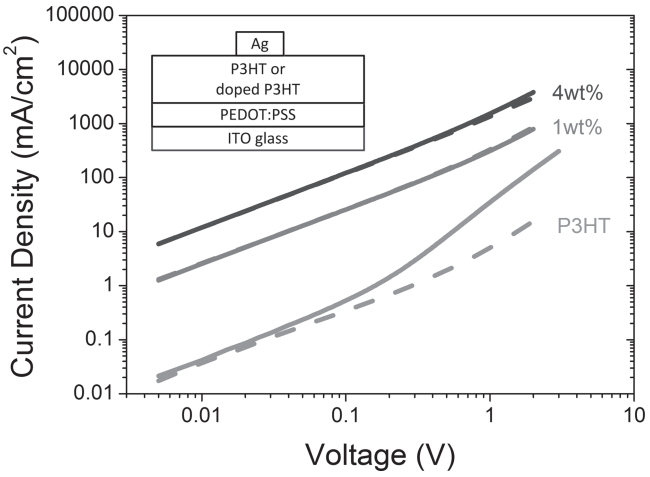

Figure 4. *J–V* characteristics of undoped and doped P3HT hole-only devices (transport perpendicular to the film). Full and dashed curves correspond to hole injection from PEDOT:PSS and Ag, respectively.

of the film increase slightly during the doping process. UPS measurements of doped P3HT films deposited on poly(3,4-ethylenedioxythiophene):poly(styrenesulfonate),PEDOT:PSS, -covered substrates yield very similar results (not shown here).

3.2. Carrier Transport

Room temperature current density–voltage (*J–V*) measurements were performed under N_2 on a series of hole-only diode structures consisting of a single 90 nm-thick layer of undoped or doped P3HT sandwiched between PEDOT:PSS (AI 4083) and a Ag contact. In these measurements, carrier transport is perpendicular to the P3HT film. Bias is applied to the Ag electrode while the ITO/PEDOT:PSS substrate is grounded. Electron injection from PEDOT:PSS or Ag can be neglected given the large energy barrier formed on either side with the P3HT LUMO (EA of P3HT = ca. 2.15 eV).[32] Room-temperature *J–V* characteristics as a function of doping concentrations are given in **Figure 4**, with the full and dotted curves corresponding to holes injected from the PEDOT:PSS and Ag, respectively. Current in undoped P3HT (black) is in the Ohmic regime below 0.1 V ($J\alpha V$), regardless of whether holes are injected from PEDOT:PSS or Ag. Parasitic leakage currents also likely contribute to the current in this bias regime. The two curves (full and dotted) diverge above 0.1 V, consistent with the expectation that hole-injection from PEDOT:PSS is more efficient than from Ag. The current then approaches the space-charge-limited current (SCLC) regime ($J\alpha V^2$).

The current density for a film doped at 4 wt% of Mo(tfd-CO_2Me)$_3$ is more than two orders-of-magnitude larger than that for an undoped film. Doping also eliminates the difference between hole-injection from the two different electrodes in this bias window. As mentioned above, a higher hole-injection barrier is expected for Ag, due to its lower WF and other issues related to clean metal contacts, such as the push back/pillow effect,[6] yet, doping is known to lower the effective injection barrier, by changing the molecular level alignment at the interface[33] and/or creating a narrow depletion region at the interface through which carriers can tunnel.[4,34]

Lateral transport was also investigated on films spin-coated on quartz substrates patterned with inter-digitated gold electrodes. These measurements were performed in vacuum, at low field (< 3×10^3 V cm^{-1}), as a function of doping and temperature (110–350 K). The conductivity σ of each sample, determined from the Ohmic region of the *I–V* characteristics and the known film thickness, is plotted in **Figure 5** on a logarithmic scale versus $1/T$. σ follows an Arrhenius relationship with temperature, $\sigma = \sigma_0 e^{-E_{act}/kT}$, where σ_0 is a pre-factor and E_{act} is the activation energy of the charge carrier hopping process. As has been previously observed for other doped organic films,[35,36] σ increases by several orders of magnitude as more dopants are introduced in the host film.

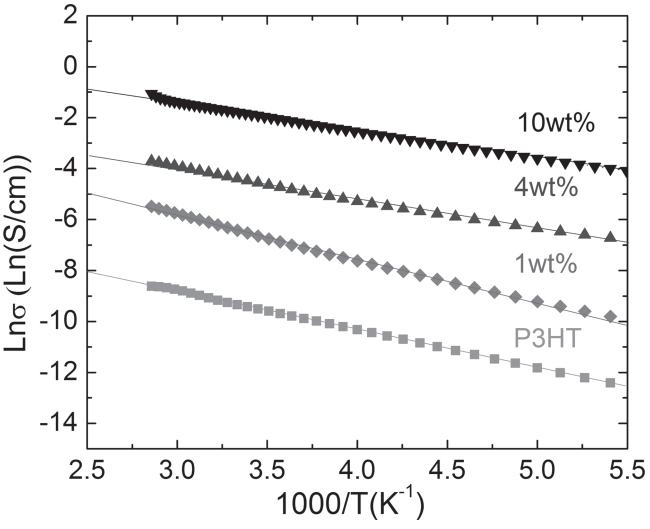

Figure 5. Conductivity extracted from the variable temperature *J–V* data (transport parallel to the film), plotted on a log scale as a function of temperature.

In summary, both sets of current-voltage measurements show that the new dopant Mo(tfd-$CO_2Me)_3$ is readily dissolved within the P3HT solution and effectively p-dopes the polymer. In the remainder of this work, the dopant is used to p-dope polymer films to be transferred and laminated to achieve low resistance hole-injection or hole-collection contacts.

4. Transfer-Lamination of Doped Polymer Films

We now consider the formation of doped contacts to undoped P3HT via SCTL of doped films on top of undoped P3HT, and the impact on carrier injection at the organic polymer/metal interface of hole-only devices. The SCTL procedure has been detailed elsewhere[29] and is briefly described in the experimental section.

Control devices were made with the following structure: ITO/PEIE/P3HT(150 nm)/Ag, in which P3HT is spin-coated under standard conditions and PEIE (polyethylenimine ethoxylated)[3] is used to lower the ITO WF and ensure that no holes can be injected from that electrode. Laminated devices (inset in **Figure 6**) had the following structure: ITO/PEIE/P3HT(150nm)/P3HT(30nm):Mo(tfd-$CO_2Me)_3$ (0 to 10 wt%)/Ag, in which the top p-doped P3HT layer is laminated, thereby inserting a thin doped layer between the subsequently evaporated Ag contact and the undoped P3HT film.

J–V characteristics of these devices, recorded in inert atmosphere, are shown in Figure 6. UPS measurements indicate that ITO/PEIE has a WF of 3.6 eV,[3] while the WF of clean Ag is ≈ 4.3 eV.[37] On the ITO/PEIE side, the energy barrier for hole injection is large (>1 eV from UPS measurements, not shown here), and no significant hole-injection is expected when that side is biased positively. Similarly, the electron-injection barrier on the Ag side is large, given the 4.3 eV metal WF and the 2.15 eV P3HT EA.[32] The reverse bias current (negative bias in Figure 6), therefore, remains very low, independently of the structure of the device.

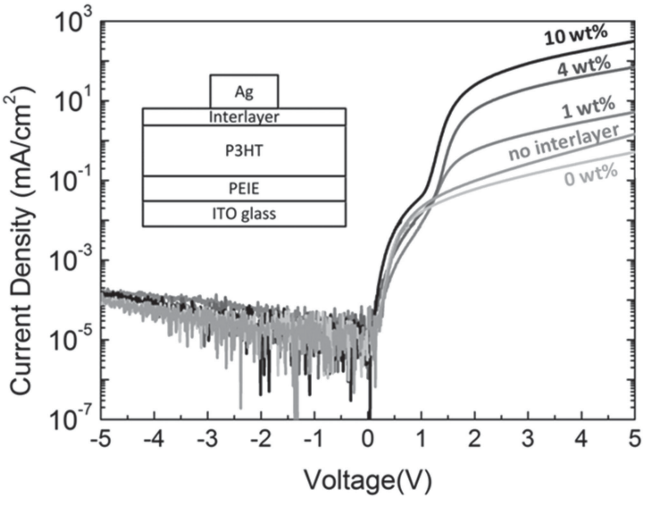

Figure 6. *J–V* characteristics of devices without and with laminated layer. The laminated layer is either undoped (0 wt%), or doped at 1, 4, or 10 wt%.

In forward bias (positive on Ag), hole injection from Ag dominates the current. The electron current injected from the PEIE side is still expected to be negligible, given the difference between the ITO/PEIE WF (3.6 eV) and the P3HT electron affinity (2.15 eV). On the other hand, the hole injection barrier on the Ag side should be significantly below 1 eV, even for undoped P3HT. As mentioned above, in the Ohmic regime (<0.5 V), the current is likely a combination of transport of bulk carriers and parasitic leakage currents. The current of the control devices (single undoped P3HT layer and laminated undoped P3HT/P3HT double layer) overlaps with those of the laminated P3HT/doped P3HT devices, which confirms that the conductivity of the P3HT structure is not significantly changed by the presence of the laminated doped P3HT layer (considering the large thickness ratio between the two layers). As the bias increases, injected carriers begin to dominate revealing the effect of the doped laminated layer. Above 1.5 V, the current increases drastically with the doping concentration. Above 2 V and with a 10 wt% dopant concentration, the current is nearly three orders-of-magnitude larger than for the undoped control device, which is attributable to a dramatic improvement in hole-injection from the Ag side. This phenomenon has been observed in several small-molecule systems where control of vacuum evaporation permits the localization of dopants in the immediate vicinity of the electrode-organic interface,[4,38] and has been attributed either to a shift of the organic molecular levels with respect to the Fermi level of the contacts and/or to the formation of a narrow depletion region in the semiconductor, both of which can lead to a lowering of the effective injection barrier. In the present case, the thin doped laminated P3HT layer plays an identical role, effectively lowering the injection barrier without altering the electronic properties of the bulk semiconductor layer of the device.

5. Solar Cells with Transfer-Laminated Doped Layer as Hole-Collecting Contact

In order to extend this method to device application, we combine the concept of spatially-confined molecular doping with the SCTL technique to create efficient hole-collecting contacts on bulk heterojunction (BHJ) solar cells. The multilayer inverted solar cells have the following layer sequence: i) a PEIE-modified ITO substrate for electron collection; ii) a P3HT:6,6-phenyl-C_{61}-butyric acid methyl ester (PCBM) or P3HT:indene-C_{60} bis-adduct (ICBA) active layer; iii) an interlayer consisting of either PEDOT:PSS CPP, undoped P3HT, or P3HT p-doped with 1 or 4 wt% Mo(tfd-$CO_2Me)_3$; and iv) a Ag contact. The PEDOT:PSS CPP interlayer was spin-coated directly on the active layer and post annealed, while the undoped and doped P3HT layers were laminated onto the active layer.

The structures of solar cells (A through J) with different geometry and their photovoltaic parameters measured at 1 sun under AM 1.5 illumination are summarized in **Table 1**. For reference, devices without interlayer in which the top Ag electrode was directly evaporated on top of the active layer were also fabricated. Such reference devices (device A with P3HT:PCBM and device F with P3HT:ICBA) showed poor rectification in the dark and yielded low photovoltaic performance. With the

Table 1. Solar cell performance.

Device	Structure	V_{oc} [V]	J_{sc} [mA cm^{-2}]	FF	Efficiency [%]
A	ITO/PEIE/P3HT:PCBM/Ag	0.055 ± 0.003	4.0 ± 0.1	0.24 ± 0.02	0.05 ± 0.01
B	ITO/PEIE/P3HT:PCBM/P3HT/Ag	0.33 ± 0.03	4.0 ± 0.2	0.15 ± 0.01	0.21 ± 0.02
C	ITO/PEIE/P3HT:PCBM/1 wt% dp P3HT/Ag	0.55 ± 0.02	8.4 ± 0.3	0.40 ± 0.01	1.8 ± 0.1
D	ITO/PEIE/P3HT:PCBM/4 wt% dp P3HT/Ag	0.56 ± 0.01	8.0 ± 0.2	0.64 ± 0.01	2.9 ± 0.1
E	ITO/PEIE/P3HT:PCBM/PEDOT:PSS CPP/Ag	0.57 ± 0.01	8.7 ± 0.1	0.58 ± 0.01	2.9 ± 0.1
F	ITO/PEIE/P3HT:ICBA/Ag	0.18 ± 0.01	6.7 ± 1.6	0.31 ± 0.01	0.37 ± 0.10
G	ITO/PEIE/P3HT:ICBA/P3HT/Ag	0.50 ± 0.03	4.0 ± 0.3	0.12 ± 0.03	0.24 ± 0.02
H	ITO/PEIE/P3HT:ICBA/1 wt% dp P3HT/Ag	0.79 ± 0.01	7.5 ± 0.6	0.35 ± 0.02	2.1 ± 0.3
I	ITO/PEIE/P3HT:ICBA/4 wt% dp P3HT/Ag	0.80 ± 0.01	7.7 ± 0.3	0.63 ± 0.01	3.9 ± 0.2
J	ITO/PEIE/P3HT:ICBA/PEDOT:PSS CPP/Ag	0.79 ± 0.01	9.2 ± 0.4	0.56 ± 0.02	4.0 ± 0.3

introduction of a transfer-laminated undoped P3HT interlayer (device B with P3HT:PCBM and device G with P3HT:ICBA) the devices show strong rectification in the dark but the *J–V* characteristics under illumination exhibit an S-shaped kink as shown in **Figures 7**a, **8**a. As shown previously,[19] the existence of an S-shaped kink in the *J–V* characteristics under illumination can be correlated with the limited difference in WF between the two electrodes in the solar cell. It was observed that the S-shaped kink could be removed by either reducing the WF of the electron-collecting electrode, or by increasing that of the hole-collecting contact through UV illumination. In this study, as discussed above, the WF of the hole collecting interlayer can be increased by means of doping.

For both devices C (Figure 7a) and H (Figure 8a), which use different active layers, the introduction of a 1 wt% doped P3HT interlayer leads to a significant improvement in the shape of the *J–V* characteristics. As shown above, doping induces a shift of the WF from 4.0 eV (undoped P3HT) to 4.15 eV (1 wt% doped P3HT), which increases the difference in WF between the two electrodes and the built-in potential in the solar cell. The open-circuit voltage values for both devices C and H (see Table 1) are significantly increased compared with devices with undoped P3HT interlayers but the fill-factors are still low because the S-shaped kink is still partially present.

Further increasing the value of the WF of the hole-collecting electrode by use of a 4 wt% doping level in the P3HT interlayer entirely eliminates the S-shaped kink in the *J–V* characteristics, yielding devices (device D in Figure 7a and device I in Figure 8a) with typical simple diode-like shapes and good performance (see Table 1). By increasing the doping level in the P3HT interlayer from 1 to 4 wt%, the Fermi level further drops from 4.15 eV to 4.26 eV below vacuum level. To calibrate the performance of these solar cells, reference devices with a top PEDOT:PSS CPP interlayer were also fabricated (device E with P3HT:PCBM and device J with P3HT:ICBA). As shown in Figures 7a, 8a, and Table 1, the performance of devices D and I using 4 wt% doped P3HT interlayers is comparable to that of reference devices E and J, respectively, using PEDOT:PSS CPP. In particular, the V_{OC} values are in the range of the typical values reported for P3HT:PCBM and P3HT:ICBA solar cells.[39,40] In all these

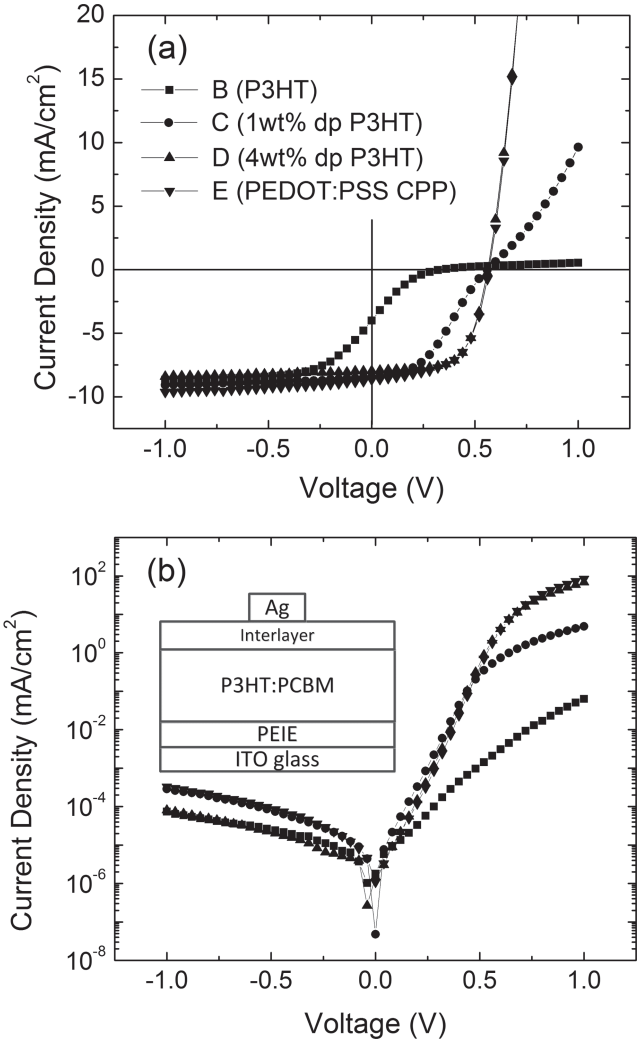

Figure 7. a) *J–V* characteristics of polymer solar cells with P3HT:PCBM bulk heterojunction under AM1.5 illumination (100 mW cm^{-2}); b) Dark *J–V* characteristics of polymer solar cells with P3HT:PCBM bulk heterojunction.

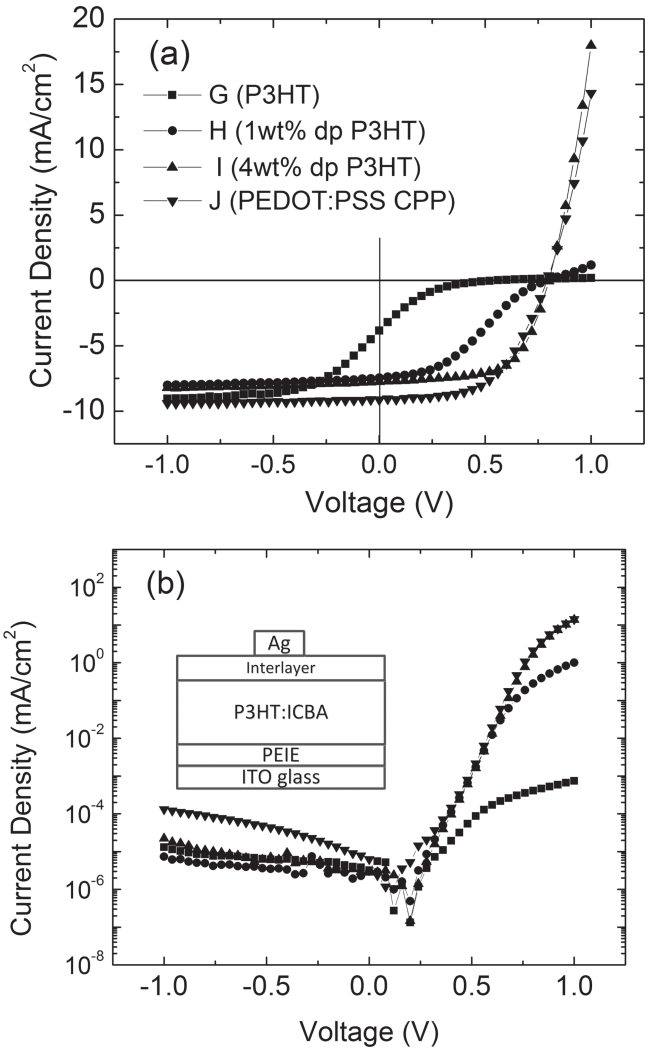

Figure 8. a) *J–V* characteristics of polymer solar cells with P3HT:ICBA bulk heterojunction under AM1.5 illumination (100 mW cm^{-2}); b) Dark *J–V* characteristics of polymer solar cells with P3HT:ICBA bulk heterojunction.

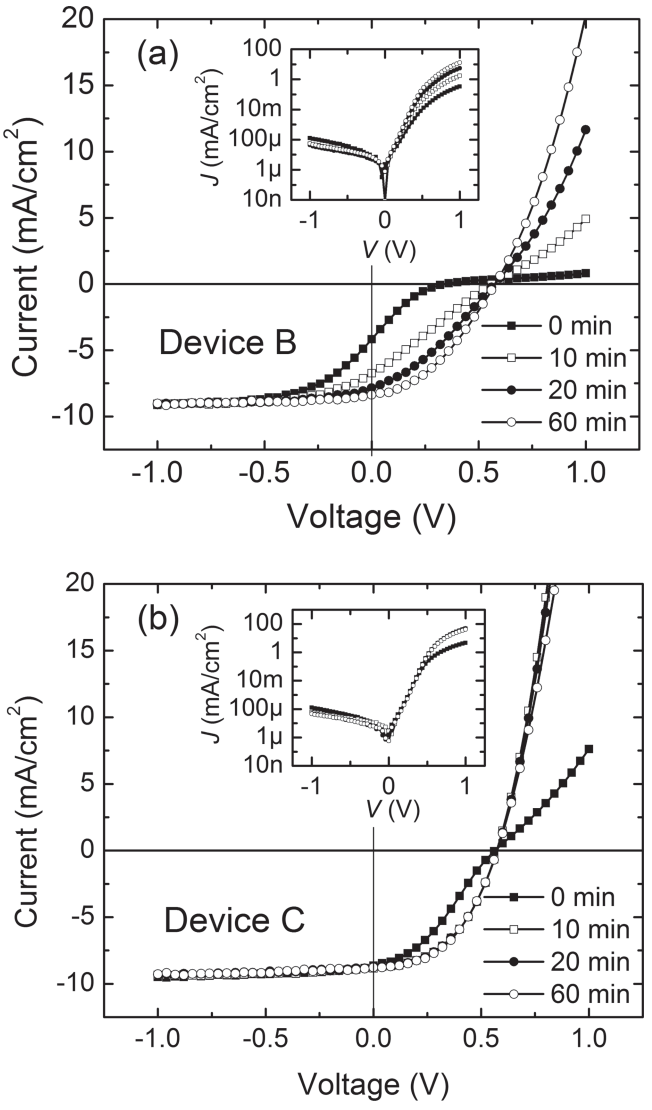

Figure 9. a) *J–V* characteristics of device B with 0, 10, 20, 60 min exposure time to air under AM1.5 illumination (100 mW cm^{-2}); b) same as (a), for device C. Insets show the dark *J–V* characteristics.

devices, the laminated P3HT interlayer keeps the reverse dark current notably low and, except for device C, lower by a factor of 5–10 than the PEDOT:PSS interlayer.

The WF of Ag is known to increase with exposure to air due to the formation of the higher WF AgO_x(5.3 eV).[37] This property offers an independent way to study the correlation between the existence and removal of an S-shaped kink in the *J–V* characteristics and the values of the WF of the electrodes in our devices. Hence, experiments were carried out whereby solar cells with two different geometries were exposed to air for specific amounts of time. As shown in **Figure 9**a for device B and Figure 9b for device C, the S-shaped kink gradually disappears with increasing continuous exposure to air. In device B with an undoped P3HT interlayer, it takes about 60 min to eliminate completely the kink, while in device C with a 1 wt% doped P3HT interlayer, the kink has disappeared after only 10 min. These data suggest that if the value of the WF of the interlayer is too low, as is the case for undoped and 1 wt% doped P3HT, the built-in potential in the device can be further increased by increasing the WF of the electrode in contact with the interlayer, in this case by increasing the WF for Ag through oxidation.

6. Conclusion

We have presented a new and highly versatile method for introducing spatially-confined chemical doping into polymer structures processed from solution. Transfer and soft-contact lamination of thin doped polymer layers (≈30 nm) allows unprecedented flexibility in the positioning of the doped region and leads to the formation of efficient low-resistance contacts to polymer films without affecting the electronic properties of the rest of the polymer structure. In the present case, p-doping of the laminated polymer layer was realized with a new soluble highly oxidizing molecule, $Mo(tfd\text{-}CO_2Me)_3$. We demonstrated

significant improvement in hole-injection in an undoped P3HT film through a thin doped contact. Finally, we used soft-contact lamination of a series of thin p-doped P3HT films on the active region of P3HT:PCBM and P3HT:ICBA bulk-heterojunction solar cells, and demonstrated that they function as efficient hole-collecting electrodes.

7. Experimental Section

Synthesis of $(NEt_4^+)_2[Mo(tfd\text{-}CO_2Me)_3]^{2-}$: $CF_3C{\equiv}CCO_2Me$ (10.0 g, 65.8 mmol)[30] was added to a stirred suspension of $(NEt_4^+)_2[MoS_9]^{2-}$[31](10.0 g, 15.5 mmol) in CH_3CN (180 mL) by syringe at 0 °C. The reaction mixture was allowed to warm to room temperature; after 1 h at room temperature the mixture was heated to 60 °C overnight, during which time the color changed from red-brown to dark green-blue. The dark green residue was extracted with dichloromethane (200 mL) and filtered. Methanol (600 mL) was added into dichloromethane solution and the dichloromethane carefully removed under reduced pressure; the remaining solution was cooled to –80 °C overnight. The resultant dark-blue semi-solid was isolated. After further purification by repetition of this extraction/precipitation process six times, and dyring of the final solid under vacuum, an analytically pure dark-blue solid (7.0 g, 45%) was obtained. ^{1}H NMR (400 MHz, CD_3CN): δ 3.78 (s, 9H, OCH_3), 3.13 (q, J_{HH} = 7.2 Hz, 16H, NEt_4CH_2), 1.20 (t of 1:1:1 t, J_{HH} = 7.2 Hz, J_{HN} = ca. 2 Hz, 3H, NEt_4CH_3). ^{19}F NMR (376.5 MHz, CD_3CN): δ –55.74 (s, CF_3). $^{13}C\{^1H\}$NMR (100 MHz, CD_3CN): 169.52 (*C*O), 148.01(s, *C*SCO), 139.27 (q, J_{CF} = 31 Hz, *C*SCF_3), 123.87 (q, J_{CF} = 269 Hz, CF_3), 52.07 (1:1:1 t, J_{CN} = 3 Hz, NEt_4CH_2), 52.00 (s, OCH_3), 6.66 ppm8.03 (NEt_4CH_3). Anal. calcd for $C_{31}H_{49}F_9N_2O_6S_6Mo$: C 37.04, H 4.91, N 2.78, S 19.14, F 17.01. Found: C 36.49, H 4.65, N 2.78, S 19.60, F 17.01. MALDI-MS: *m/z* 745.9 ($[M–2NEt_4]^-$).

Synthesis of $Mo(tfd\text{-}CO_2Me)_3$: Excess $NOPF_6$ (850 mg, 4.88 mmol) was added to a solution of $(NEt_4^+)_2[Mo(tfd\text{-}CO_2Me)_3]^{2-}$(1.00 g, 0.995 mmol) in CH_2Cl_2 (20 mL) and the reaction was stirred under nitrogen at room temperature overnight, over which time the color of the solution turned from dark green to dark blue. The volatiles were removed under reduced pressure and the solid was extracted in hexane. Evaporation of the hexane extracts gave a dark blue crystalline solid; impurities were removed by sublimation (ca. 75–95 °C, ca. 20 mTorr; the product itself can be sublimed at higher temperature, but this is not necessary to obtain pure product) and washing with pentane (430 mg, 58%). ^{1}H NMR (400 MHz, $CDCl_3$): δ 3.99 (s, OCH_3). ^{19}F NMR (376.5 MHz, $CDCl_3$): δ –56.58 (s, CF_3). $^{13}C\{^1H\}$ NMR (100 MHz, $CDCl_3$): δ 168.76 (s, *C*O), 163.59 (q, J_{CF} = 36 Hz, *C*SCF_3), 163.31 (s, *C*SCO), 121.50 (q, J_{CF} = 275 Hz, CF_3), 54.34 (s, OCH_3). Anal. calcd for $C_{15}H_9F_9O_6S_6Mo$: C 24.20, H 1.22, S 25.84. Found: C 24.23, H 1.11, S 25.60. EI-MS: *m/z* 745.8 (M^+).

Sample Fabrication: The IE and EA of $Mo(tfd\text{-}CO_2Me)_3$ were determined via UPS and IPES on an 8 nm film of the molecule spin-coated from chlorobenzene (8 mg mL^{-1}) under N_2 onto a Si wafer covered with a 10-nm Ti adhesion layer and a 100 nm Au layer. Prior to spin-coating, the substrates were cleaned in ultrasonic baths of acetone and isopropanol for 15 min each, followed by a 10 min UV-ozone treatment. Subsequent to spin-coating, the sample was introduced in the photoemission analysis chamber without further exposure to air. Both He(I) and He(II) photon lines (21.22 and 40.81 eV, respectively) from a He discharge lamp were used as radiation lines for UPS. The resolution for the UPS measurements was 0.15 eV. IPES was performed in the isochromat mode using a set-up and a procedure described elsewhere.[41] The resolution of the IPES measurements was 0.45 eV. The calibration of both experiments, and the alignment of the two energy scales were performed using the Fermi step measured on a clean Au surface. The position of the vacuum level (E_{vac}) was determined for each sample from the energy of the photoemission cutoff, following a well-established procedure.[42]

Doped P3HT films were spin-coated from a co-solution of host and dopant in N_2. P3HT (Merck Chemicals Ltd.) was dissolved in chlorobenzene (10–30 mg mL^{-1}) and stirred at 45 °C for 4 h. $Mo(tfd\text{-}CO_2Me)_3$ was also dissolved in chlorobenzene (2–4 mg mL^{-1}). Different doping concentrations were achieved by mixing appropriate amounts of the two solutions, followed by 1 h stirring at 45 °C. The mixed solution was then spin-coated onto the substrate in N_2, annealed at 110 °C for 10 min and transferred without ambient exposure to the vacuum system for UPS analysis. Undoped or doped P3HT films for UPS analysis were spin-coated onto ITO substrates cleaned as described above, and had a thickness of ≈ 20 nm.

Two types of devices were made for transport measurements. Diode-type structures for perpendicular transport measurements were made with films spin-coated under the conditions described above onto ITO covered with a layer of PEDOT:PSS. ITO substrates were sequentially sonicated in Alconox,acetone, and isopropanol (15 min each), and UV-ozone treated for 10 min. PEDOT:PSS was spin-coated at 5000 rpm for 30 s to create a 40 nm film and annealed at 160 °C on a hot plate for 5 min. Undoped or doped P3HT films were deposited by spin-coating an appropriately mixed host-dopant co-solution (ca. 20 mg mL^{-1} chlorobenzene) at 1500 rpm for 40 s, giving ≈ 90 nm thick films. Arrays of 1 mm^2 top Ag contacts were evaporated in a vacuum chamber through a shadow mask. Devices for lateral transport measurements were made by spin-coating undoped or doped P3HT on quartz slides patterned with inter-digitated gold electrodes, with inter-electrode gaps of 150 µm.[35] The data presented in Figures 4, 6 are all representative of *J–V* curves measured on 4 to 6 devices, depending on doping.

Soft-Contact Transfer Lamination (SCTL) Process: The polymer layer (doped or undoped) to be transferred via lamination was initially spun in N_2 onto a UV-ozone exposed silicon substrate, with no subsequent annealing. A polydimethylsiloxane (PDMS) stamp was placed in contact with the top of the polymer film, and the assembly submerged in DI water for 1 min to delaminate the polymer film from the hydrophilic SiO_2 surface. The delaminated top polymer film was then brought into contact with the other spin-coated (bottom) polymer film, and the PDMS stamp was removed. No annealing was performed.

Solar Cell Devices: The active layers consisted of P3HT as donor and PCBM or ICBA as acceptor. 10 nm PEIE was spin-coated on the pre-patterned ITO substrate. Donor and acceptor materials were mixed in 1,2-dichlorobenzene with 1:1 weight ratio (40 mg mL^{-1}) and 200 nm bulk-heterojunction films were deposited onto the PEIE-modified ITO substrates by spin-coating (1000 rpm for 60 s). The active layer was solvent-annealed overnight, and then annealed on a hot plate at 150 °C for 10 min in N_2. The interlayers (P3HT, 1 wt% doped P3HT and 4 wt% doped P3HT) were first spin-coated onto a plasma treated Si substrate, then transferred to PDMS stamp and attached to the active layer with SCTL. For the deposition of interlayer PEDOT:PSS (CPP), a 40 nm film was directly spin-coated onto the active layers and the whole assembly was subsequently annealed at 120 °C for 10 min. All the samples were then loaded into a vacuum thermal evaporator (EvoVac, Angstrom Engineering Inc.), and 100 nm of Ag were deposited through a shadow mask at a base pressure of 2×10^{-7} Torr. The effective area of the active layer was 10 mm^2.

Current density-voltage (*J-V*) characteristics of the solar cells were measured in a N_2-filled glovebox with a source meter (2400, Keithley Instruments, Cleveland, OH) controlled by a LabVIEW program. An Oriel lamp with an air mass 1.5 filter and an intensity of 100 mW cm^{-2} was used as the light source. The data presented in Figures 7, 8 are all representative of *J–V* curves measured on 3 to 9 devices, depending on structure and interlayer doping.

Acknowledgements

Support of this work at Princeton was through the Princeton MRSEC of the National Science Foundation (DMR-0819860) and a grant of the

National Science Foundation (DMR-1005892). Research done at the Georgia Institute of Technology was supported in part by the Center for Interface Science: Solar-Electric Materials (CIS:SEM), an Energy Frontier Research Center funded through the U.S. Department of Energy, Office of Basic Energy Sciences, under Award Number DE-SC0001084 (for development of procedures for efficient synthesis of dopants), by the U.S. Department of Energy through the Bay Area Photovoltaic Consortium under Award Number DE-EE0004946, and by the Office of Naval Research (N00014–11–1–0313, for the initial studies on the development of the Mo dopant used in this paper).

Received: September 18, 2013
Published online: December 17, 2013

[1] L.-M. Chen, Z. Xu, Z. Hong, Y. Yang, *J. Mater. Chem.* **2010**, *20*, 2575.
[2] K. Fehse, S. Olthof, K. Walzer, K. Leo, R. L. Johnson, H. Glowatzki, B. Broker, N. Koch, *J. Appl. Phys.* **2007**, *102*, 073719.
[3] Y. Zhou, C. Fuentes-Hernandez, J. Shim, J. Meyer, A. J. Giordano, H. Li, P. Winget, T. Papadopoulos, H. Cheun, J. Kim, M. Fenoll, A. Dindar, W. Haske, E. Najafabadi, T. M. Khan, H. Sojoudi, S. Barlow, S. Graham, J.-L. Bredas, S. R. Marder, A. Kahn, B. Kippelen, *Science* **2012**, *336*, 327.
[4] Y. Qi, T. Sajoto, M. Kroger, A. M. Kandabarow, W. Park, S. Barlow, E.-G. Kim, L. Wielunski, L. C. Feldman, R. A. Bartynski, J.-L. Bredas, S. R. Marder, A. Kahn, *Chem. Mater.* **2009**, *22*, 524.
[5] S. Braun, W. R. Salaneck, M. Fahlman, *Adv. Mater.* **2009**, *21*, 1450.
[6] A. Kahn, N. Koch, W. Gao, *J. Polym. Sci. Part B: Polym. Phys.* **2003**, *41*, 2529.
[7] Y. Shen, A. R. Hosseini, M. H. Wong, G. G. Malliaras, *ChemPhys Chem* **2004**, *5*, 16.
[8] J. W. Shim, H. Cheun, J. Meyer, C. Fuentes-Hernandez, A. Dindar, Y. H. Zhou, D. K. Hwang, A. Kahn, B. Kippelen, *Appl. Phys. Lett.* **2012**, *101*, 073303.
[9] Y. Zhou, J. W. Shim, C. Fuentes-Hernandez, A. Sharma, K. A. Knauer, A. J. Giordano, S. R. Marder, B. Kippelen, *Phys. Chem. Chem. Phys.* **2012**, *14*, 12014.
[10] B. Zacher, J. L. Gantz, R. E. Richards, N. R. Armstrong, *J. Phys. Chem. Lett.* **2013**, *4*, 1949.
[11] S. M. Sze, *Phys. Semicond. Devices* 2nd Edition, John Wiley & Sons, New York 1981.
[12] C. Falkenberg, C. Uhrich, S. Olthof, B. Maennig, M. K. Riede, K. Leo, *J. Appl. Phys.* **2008**, *104*, 034506.
[13] C. Uhrich, D. Wynands, S. Olthof, M. K. Riede, K. Leo, S. Sonntag, B. Maennig, M. Pfeiffer, *J. Appl. Phys.* **2008**, *104*, 043107.
[14] Y. Wang, W. Gao, S. Braun, W. R. Salaneck, F. Amy, C. Chan, A. Kahn, *Appl. Phys. Lett.* **2005**, *87*, 193501.
[15] G. He, O. Schneider, D. Qin, X. Zhou, M. Pfeiffer, K. Leo, *J. Appl. Phys.* **2004**, *95*, 5773.
[16] J. Huang, M. Pfeiffer, A. Werner, J. Blochwitz, K. Leo, S. Liu, *Appl. Phys. Lett.* **2002**, *80*, 139.
[17] S. Olthof, S. Singh, S. K. Mohapatra, S. Barlow, S. R. Marder, B. Kippelen, A. Kahn, *Appl. Phys. Lett.* **2012**, *101*, 253303.
[18] B. H. Hamadani, H. Ding, Y. Gao, D. Natelson, *Phys. Rev. B* **2005**, *72*, 235302.
[19] W. Tress, K. Leo, M. Riede, *Adv. Funct. Mater.* **2011**, *21*, 2140.
[20] Y.-L. Loo, T. Someya, K. W. Baldwin, Z. Bao, P. Ho, A. Dodabalapur, H. E. Katz, J. A. Rogers, *Proc. Natl. Acad. Sci.* **2002**, *99*, 10252.
[21] J. Zaumseil, K. W. Baldwin, J. A. Rogers, *J. Appl. Phys.* **2003**, *93*, 6117.
[22] M. L. Chabinyc, A. Salleo, Y. Wu, P. Liu, B. S. Ong, M. Heeney, I. McCulloch, *J. Am. Chem. Soc.* **2004**, *126*, 13928.
[23] S. K. Park, K. Yong Hoon, J.-I. Han, M. Dae Gyu, K. Won Keun, *IEEE Trans. Electron Dev.* **2002**, *49*, 2008.
[24] H. Wang, E. D. Gomez, J. Kim, Z. Guan, C. Jaye, D. A. Fischer, A. Kahn, Y.-L. Loo, *Chem. Mater.* **2011**, *23*, 2020.
[25] H. Wang, M. Shah, V. Ganesan, M. L. Chabinyc, Y.-L. Loo, *Adv. Energy Mater.* **2012**, *2*, 1447.
[26] J. B. Kim, Z.-L. Guan, S. Lee, E. Pavlopoulou, M. F. Toney, A. Kahn, Y.-L. Loo, *Org. Electron.* **2011**, *12*, 1963.
[27] J. B. Kim, Z.-L. Guan, A. L. Shu, A. Kahn, Y.-L. Loo, *Langmuir* **2011**, *27*, 11265.
[28] J. B. Kim, S. Lee, M. F. Toney, Z. Chen, A. Facchetti, Y. S. Kim, Y.-L. Loo, *Chem. Mater.* **2010**, *22*, 4931.
[29] A. L. Shu, A. Dai, H. Wang, Y.-L. Loo, A. Kahn, *Org. Electron.* **2012**, *14*, 149.
[30] P. Jeannin, M. Fourmigué, *Chem. Eur. J.* **2006**, *12*, 2994.
[31] M. Draganjac, E. Simhon, L. T. Chan, M. Kanatzidis, N. C. Baenziger, D. Coucouvanis, *Inorg. Chem.* **1982**, *21*, 3321.
[32] Z.-L. Guan, J. B. Kim, H. Wang, C. Jaye, D. A. Fischer, Y.-L. Loo, A. Kahn, *Org. Electron.* **2010**, *11*, 1779.
[33] W. Gao, A. Kahn, *J. Phys.: Condens. Matter* **2003**, *15*, S2757.
[34] W. Gao, A. Kahn, *Org. Electron.* **2002**, *3*, 53.
[35] S. Olthof, S. Mehraeen, S. K. Mohapatra, S. Barlow, V. Coropceanu, J.-L. Bredas, S. R. Marder, A. Kahn, *Phys. Rev. Lett.* **2012**, *109*, 176601.
[36] M. Pfeiffer, A. Beyer, T. Fritz, K. Leo, *Appl. Phys. Lett.* **1998**, *73*, 3202.
[37] J. B. Kim, C. S. Kim, Y. S. Kim, Y.-L. Loo, *Appl. Phys. Lett.* **2009**, *95*, 183301.
[38] S. Olthof, W. Tress, R. Meerheim, B. Lussem, K. Leo, *J. Appl. Phys.* **2009**, *106*, 103711.
[39] G. Zhao, Y. He, Y. Li, *Adv. Mater.* **2010**, *22*, 4355.
[40] M. Reyes-Reyes, K. Kim, D. L. Carroll, *Appl. Phys. Lett.* **2005**, *87*, 083506.
[41] Y. H. C. I. Wu, H. Sirringhaus, A. Kahn, *Chem. Phys. Lett.* **1997**, *272*, 43.
[42] D. Cahen, A. Kahn, *Adv. Mater.* **2003**, *15*, 271.